ACS Photonics

pubs.acs.org/journal/apchd5

Article

Enhanced near-Infrared Photoresponse from Nanoscale Ag-Au Alloyed Films

Lisa J. Krayer, Kevin J. Palm, Chen Gong, Alberto Torres, Cesar E. P. Villegas, Alexandre R. Rocha, Marina S. Leite, and Jeremy N. Munday*

Cite This: https://dx.doi.org/10.1021/acsphotonics.0c00140

Read Online

ACCESS | Metrics & More | Article Recommendations | Supporting Information

ABSTRACT: Alloying of metals provides a vast parameter space for tuning of material, chemical, and mechanical properties, impacting disciplines ranging from photonics and catalysis to aerospace. From an optical point-of-view, pure thin metal films yield enhanced light absorption due to their cavity effects. However, an ideal metal−semiconductor photodetector requires not only high absorption, but also long hot carrier attenuation lengths in order to efficiently collect excited carriers. Here we demonstrate that Ag-Au alloys provide an ideal model system for controlling the optical and electrical responses in nanoscale thin metal films for hot carrier photodetectors with improved performance. While pure Ag and Au have long hot carrier attenuation lengths >20 nm, their optical absorption is insufficient for high efficiency devices. Instead, we find that alloying Ag and Au enhances the absorption by ∼50% while maintaining attenuation lengths >15 nm, currently limited by grain boundary scattering, although the electron attenuation length of pure Au outperforms pure Ag as well as all of the alloys investigated here. Further, our density functional theory analysis shows that the addition of small amounts of Au to the Ag lattice significantly enhances the hot hole generation rate. Combined, these findings suggest a route to high efficiency hot carrier devices based on metallic alloying with potential applications ranging from photodetectors and sensors to improved catalytic materials.

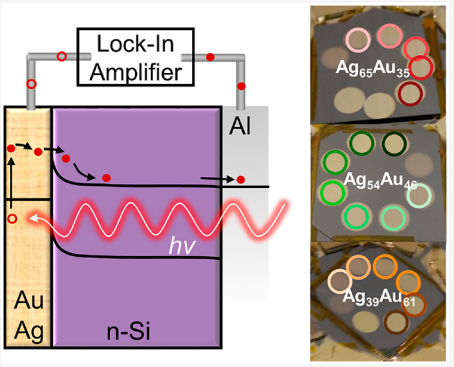

KEYWORDS: *metal alloys, hot carriers, photodetection, electron attenuation length, near-infrared absorption, Schottky photodiodes*

While the material properties of pure metals are well understood and characterized, they are not necessarily ideal for certain applications, and the ability to tune the mechanical strength, conductivity, and optical response is important for many technologies. For example, absorbing metal contacts at semiconductors junctions, Schottky photodiodes, have an incredible range of uses, including solar energy conversion,[1−3] water splitting,[4] biosensing,[5,6] and nano-optoelectronics,[7] but are limited by the predetermined response of the pure metals. For each of these applications, the metal contact needs to absorb light and subsequently generate photocurrent. Efficient photocurrent generation and collection requires (*i*) high absorption within the metal film, (*ii*) preferential carrier excitation to energy levels above the Schottky barrier height, (*iii*) lossless transport of the excited carriers to the metal interface, (*iv*) emission of the carriers over the potential barrier at the interface, and (*v*) collection of the excited carriers at an ohmic contact.[1,2,8−10] Unfortunately, pure elemental metals generally have limitations in one or more of the above-mentioned criteria, and there is thus a need for improvement through new materials development.

Au and Ag both have long electron transport attenuation lengths on the order of ∼30 nm and are commonly used to obtain high absorption by exciting plasmonic resonances. However, both metals have a peak electron density of states well below the Fermi energy, which reduces the probability that hot electrons will be excited to energies above a Schottky barrier height.[11] Further, Ag is unstable in air, and Au is not compatible with commercial semiconductor devices due to its diffusion into surrounding media at room temperature.[3,8,11,12] In addition, high absorption with Au or Ag requires nanotexturing, because their optical properties are not suitable for planar, thin film cavity resonances.[13] An alternative metal is needed that can yield more absorption, while maintaining the electrical response.

Fortunately, alloying enables tunability of the material properties ranging from structural and thermal to optical and electrical.[8,11,12,14−18] The parameter space of possible metal alloys is extensive, and the resulting material properties cannot be easily predicted. In particular, Ag-Au alloys have already been thoroughly researched for optimizing both catalytic

Received: January 29, 2020
Published: May 28, 2020

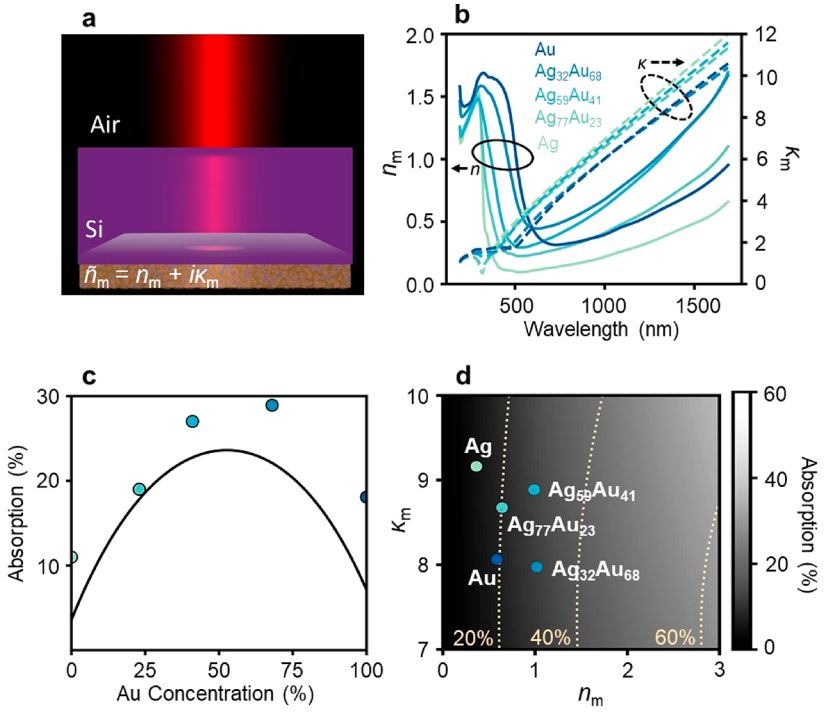

Figure 1. Optical response of Ag_xAu_{100-x} alloys compared to the pure metals. (a) Schematic showing illumination of a thin metal film with complex refractive index, $\tilde{n}_m = n_m + i\kappa_m$, through a Si substrate. (b) The measured refractive indices of each metal film. (c) Calculated absorption for varied gold concentration using optical properties determined from the analytical expression of ref 24 (black line) and the measured optical properties of the fabricated thin film alloys (circles). (d) Calculated absorption varying the optical properties of a 10 nm thin metal film. The colored dots represent the optical properties of each metal film and the dotted lines show the absorption values of 20%, 40%, and 60%.

reactions and plasmonic performance.[8,11,12,15,19−24] Au and Ag have similar lattice constants, Fermi energy, and electron effective mass; however, their optical properties and interband transition energies are different, making them prime candidates for alloying to achieve new optical responses without harming their thermal or electrical behavior.[11,22,23] Mixing Au and Ag causes a linear transition of the peak plasmon resonance and interband transition energy, but the optical properties cannot be explained by a linear combination of dielectric constants.[11,19−21,24,25] While the optical properties of Au and Ag have been recently explored, there remains a lack of understanding of how well these alloys will behave for hot carrier photodetection, particularly for near-infrared (NIR) applications.

In this manuscript, we explore the NIR optical properties and, to the best of our knowledge, are the first to characterize the photoelectrical properties of cosputtered Au and Ag alloys. We find that the alloys enhance the thin film absorption with respect to the pure metals, while maintaining similar hot carrier distributions for electrons and holes throughout the NIR spectrum. The d-band transitions significantly impact the hot carrier distributions at visible wavelengths, suggesting that hot carrier photodetectors should be designed to extract hot holes instead of hot electrons for visible photodetection. Finally, we find that the electron attenuation length (EAL) of pure Au outperforms pure Ag as well as all of the alloys investigated here, suggesting that despite low thin film absorption, pure Au remains the highest efficiency metal for hot carrier based photodetection in the NIR.

RESULTS AND DISCUSSION

Impact of Alloying on Thin Film Absorption. Illuminating a metal film through a high index material ($n > 2$) reduces reflectivity and increases absorption in nanoscale films.[13] Achieving >50% absorption requires that the thin metal film have approximately equal real and imaginary parts of the refractive indices (i.e., $n_m \sim \kappa_m$, where $\tilde{n} = n_m + i\kappa_m$) in order to satisfy the conditions for a thin film resonance. For example, it is possible to absorb >70% in a 10−20 nm metal film with $n_m \sim \kappa_m$ when illuminating the metal through a Si substrate (Figure 1a). Rioux et al. developed an analytical expression to predict the optical properties of Ag-Au alloys from the atomic percentage of Au based on their band structure.[24] From the predicted optical properties, it appears that, while pure Au and Ag do not satisfy the thin film resonance requirements for high absorption, Ag-Au alloys are likely to have higher absorption than the pure metals at NIR wavelengths because of their increased Drude dampening.[20,24]

To test this hypothesis, we sputtered thin films of Au, Ag, and Ag_xAu_{100-x}, with x = 32, 59, and 77 on Si and glass substrates for characterization (Figure 1). Energy-dispersive X-ray spectroscopy (EDS) was used to determine the alloy composition for samples on the glass substrate with an error of ±2% (see Supporting Information, Table S1). The optical properties were determined from fits to spectroscopic ellipsometry data measured for samples deposited on the glass substrate. Figure 1b shows the measured optical response of each metal film from the ultraviolent (UV) to NIR. The refractive index minimum in the near-UV shifts from Ag to Au with increasing Au concentration. This result is in agreement with the shift in transmission maximum observed by Gong[20] and is due to the progressive increase in interband transition

https://dx.doi.org/10.1021/acsphotonics.0c00140
ACS Photonics XXXX, XXX, XXX−XXX

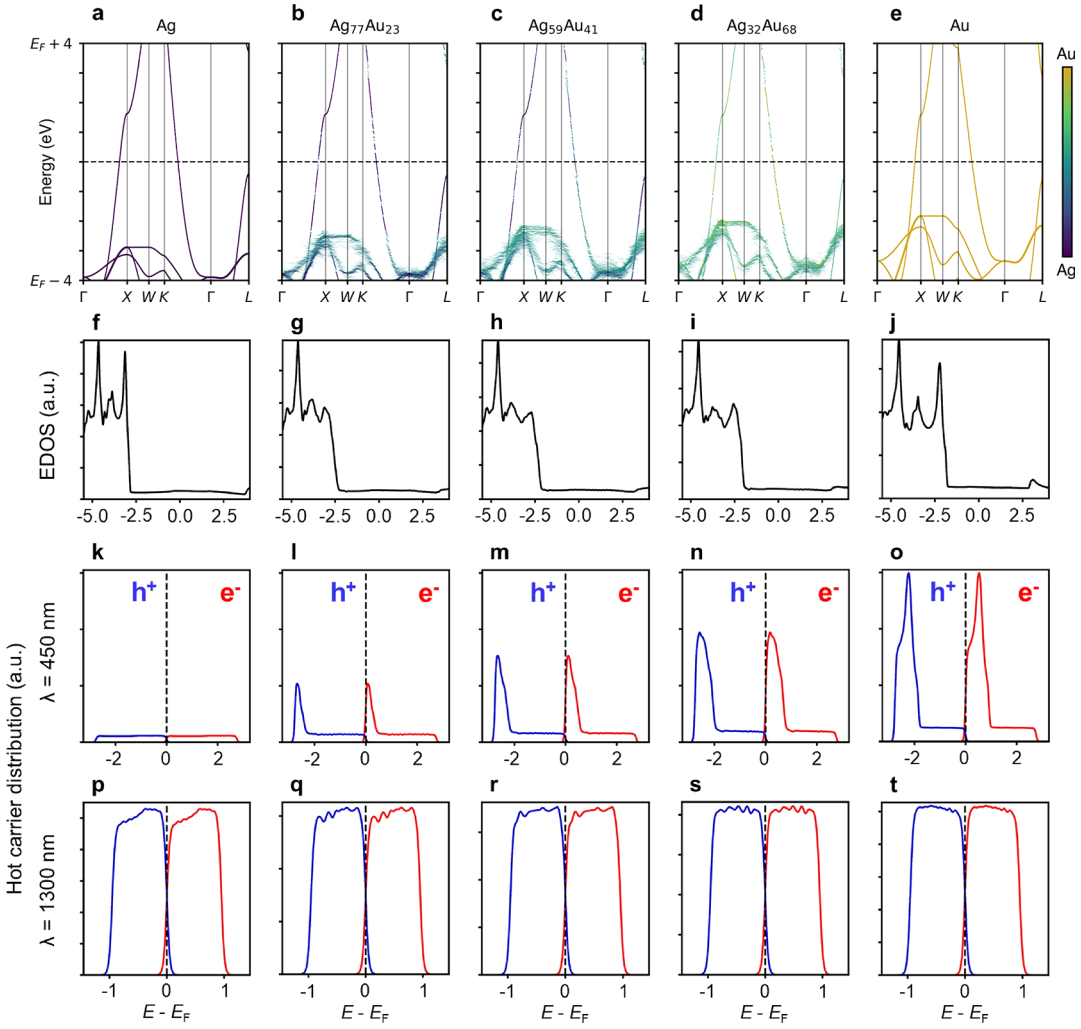

Figure 2. Density of states and hot carrier distribution in Ag_xAu_{100-x} alloys. (a–e) *k*-Dependent density of states along the *X*, Γ, and *L* Brillouin zones for an fcc lattice. The line thicknesses are determined by the density of electrons and the color shows the electron contribution from each element. (f–j) Calculated total EDOS for Au, Ag, and alloys. Hot carrier distribution for electrons (red) and holes (blue) under (k–o) 400 nm and (p–t) 1300 nm illumination.

energy with increasing Au concentration.[11,24,25] At NIR wavelengths, the optical properties no longer demonstrate this behavior, as the real part of the refractive index, n_m, for all alloys becomes larger than the pure metals beyond ∼1000 nm. The optical loss, κ_m, is also nonlinear, with Ag having the maximum and $Ag_{32}Au_{68}$ having the minimum values after ∼1000 nm. We compared the measured refractive indices with the predicted values from Rioux's model (see Supporting Information, Figure S1) and found that the measured values of n_m are larger for all the metal films in the NIR. This behavior is most likely due to an increase in Drude dampening from increased grain boundary and surface scattering with decreasing film thickness.[26]

We calculated the expected absorption for 10 nm metal films at a wavelength of 1300 nm using the transfer matrix method[27] for illumination through a silicon substrate Figure 1c shows the calculated absorption varying Au concentration using the optical properties predicted by ref[24] (black line) and our measured optical properties (circles). Based on this model, the alloy with the maximum absorption is $Ag_{53}Au_{47}$. The measured absorption in the alloys follows a similar trend; however, the absolute difference between the measured and predicted absorption is ∼10% for pure Au and $Ag_{77}Au_{23}$. By plotting the absorption versus the optical properties of the metal film (Figure 1d), we can see that the absorption increases with increasing refractive index, n_m. From Figure 1c,d, we find that all the metals absorb <30% with Ag having the lowest absorption despite having the highest optical loss. $Ag_{59}Au_{41}$ and $Ag_{32}Au_{68}$ absorb ∼20% more than Ag and ∼10% more than Au, with $Ag_{32}Au_{68}$ having the highest absorption. While all the alloys have larger absorption than the pure metals, $Ag_{77}Au_{23}$ has approximately equal absorption to Au with only a 1–2% absolute difference.

Impact of Alloying on Hot Carrier Distribution. Light absorption in the metal excites hot carriers, and the energy distribution of those carriers can be determined from the electron density of states (EDOS) and the wavelength of the incident light. Efficient hot electron collection requires the hot carriers to be excited to an energy level greater than the interfacial potential barrier (i.e., Schottky barrier). This means that the metal should have a high electron density close to the Fermi energy.[8] We calculated the reciprocal lattice dependent (i.e., *k*-dependent) EDOS for Au, Ag and alloys assuming an fcc lattice using density functional theory (DFT). The alloys were modeled with a 108-atom super cell with the arrangement of the atoms following the quasi-random structure (SQS, see

https://dx.doi.org/10.1021/acsphotonics.0c00140
ACS Photonics XXXX, XXX, XXX−XXX

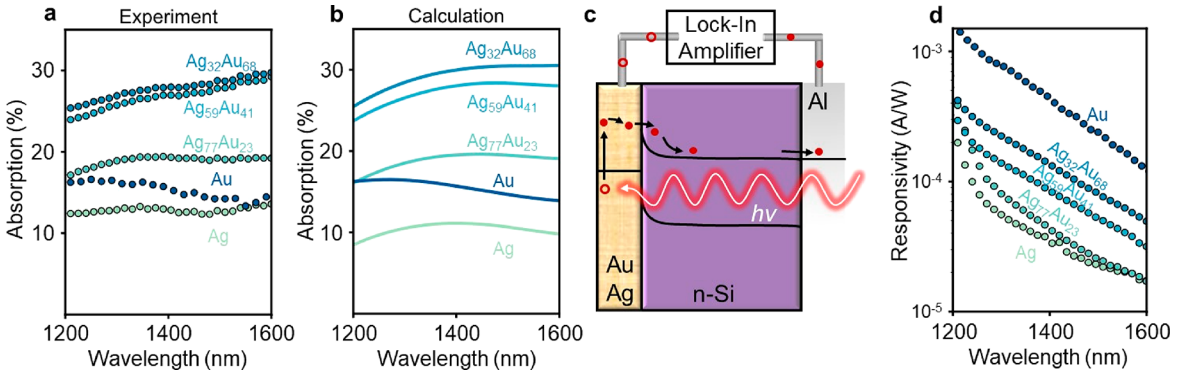

Figure 3. Absorption and photoresponse. (a) Measured and (b) calculated absorption of Au, Ag, and Ag_xAu_{100-x} metal films when illuminated through a Si substrate. (c) Band diagram of the Ag_xAu_{100-x} Schottky photodiodes. Sub-bandgap photons (i.e., $h\nu < E_g$) are absorbed in the back metal contact and excite hot electrons. The electrons travel to the interface, are injected into the *n*-Si substrate and are collected at the Al ohmic contact. (d) Measured photoresponse of all photodiodes. The photoresponse is measured using a lock-in amplifier and is calculated by dividing the current at zero applied bias under monochromatic illumination by the power from the incident photon flux.

Supporting Information, Figure S2).[28] Au and Ag have nearly identical lattice constants and therefore all Ag-Au alloys have the same crystal structure.[22,24,29]

Figure 2a–e shows the unfolded, *k*-dependent EDOS along the Γ, *X*, *W*, *K*, and *L* symmetry points of the Brillouin zone. The thicknesses of the lines are correlated with the electron density while the color determines the electron contribution from each element. In agreement with previously reported band structures for Ag-Au alloys,[24,29] the interband transition energies are determined by the band structure at the *X* and *L* symmetry points. States above (below) Fermi energy are vacant (occupied). We find that the energy of the maximum occupied states at the *X* symmetry points is matched with the onset energy of the high density regions in the total EDOS values in Figure 2f–j. We define this onset energy as the energy below the Fermi energy (E_F), where the total EDOS is 5% of its maximum value. The onset energies are 2.86, 2.41, 2.18, 2.01, and 1.78 eV in order of increasing Au molar fraction, which are consistent with the onset binding energy of the $d_{5/2}$ bands measured from the valence band and transmission spectra of Ag-Au alloys by Gong.[29]

The joint density of states, jDOS, of electrons in a metal after absorption of a photon with energy E_{ph} is determined by

$$\mathrm{jDOS}(E) \propto D(E - E_{ph})f(E - E_{ph})D(E)[1 - f(E)] \quad (1)$$

where $f(E)$ is the Fermi distribution function and $D(E)$ is the total EDOS. Similarly, the hot hole distribution is determined by

$$\mathrm{jDOS}(E) \propto D(E)f(E)D(E + E_{ph})[1 - f(E + E_{ph})] \quad (2)$$

The hot carrier distributions, calculated for wavelengths from 300 to 1300 nm (Figure S2), for the Ag-Au metals show peaks in the distribution corresponding to carrier excitation from the *d*-band. Note that the total density of states, $D(E)$, is normalized for these calculations such that the EDOS maximum is equal to 1.

Valenti et al. measured the photoresponse of Ag-Au alloy nanoparticles on a TiO_2 substrate under visible illumination and found that Ag has the highest photoresponse despite having similar maximum absorption to pure Au and an Ag-Au alloy. They hypothesized that the discrepancy was likely because Ag has a larger interband transition energy and therefore the carriers excited by wavelengths between 400 and 600 nm are more likely to be excited to energies above the barrier height.[11]

To determine how d-band excitations impact the probability of hot carrier collection, we calculated the jDOS starting at 450 nm, which corresponds to the absorption maximum for the Ag-Au alloy nanoparticles in ref 11, Figure 2k,l. The fraction of electrons excited to an energy above the barrier height can be written as[2]

$$P(E) = \frac{\int_{\phi_B}^{E_{ph}} \mathrm{jDOS}(E)\mathrm{d}E}{\int_{0}^{E_{ph}} \mathrm{jDOS}(E)\mathrm{d}E} \quad (3)$$

where ϕ_B is the Schottky barrier height. Because of the work function difference between Au and Ag, the Schottky barrier heights for each metal cannot be expected to be the same on similar substrates.[30,31] However, for the sake of simplicity, we calculate the percentage of electrons that are excited above a barrier height of 0.6 eV for all metals. For 450 nm (i.e., visible) illumination, the percentage of electrons that will be excited above the barrier height are 78%, 46%, 35%, 33%, and 41% for Ag, $Ag_{77}Au_{23}$, $Ag_{59}Au_{41}$, $Au_{32}Au_{68}$, and Au, respectively. This confirms that the *d*-band transitions are parasitic to the photoresponsivity when collecting hot electrons (i.e., using an *n*-type substrate). Alternatively, Figure 2k,l shows that *d*-band excitations are beneficial for hot hole collection. The percentage of hot holes excited to an energy above the barrier height are 77%, 87%, 90%, 93%, and 93% for Ag, $Ag_{77}Au_{23}$, $Ag_{59}Au_{41}$, $Au_{32}Au_{68}$, and Au, respectively. This suggests that Schottky photodiodes designed to absorb photons from UV to visible should use *p*-type substrates (as opposed to *n*-type substrates) in order to collect hot holes instead of electrons.

For NIR illumination, the hot carrier distribution is roughly even across $E_F < E < E_{ph}$ for all metals with Ag and Au having a slightly favorable distribution for hot electrons and holes, respectively (Figure 2p–t). For a barrier height of 0.6 eV, under 1300 nm illumination, the probability that hot electrons will be excited to an energy above the barrier is 35–37% for all metals. Similarly, the probability for hot holes ranges from 33 to 36% for all metals. Because these values are similar, there is little difference between selecting a *p*-type or *n*-type substrate for absorption of light with energy less than the *d*-band transition.

https://dx.doi.org/10.1021/acsphotonics.0c00140
ACS Photonics XXXX, XXX, XXX–XXX

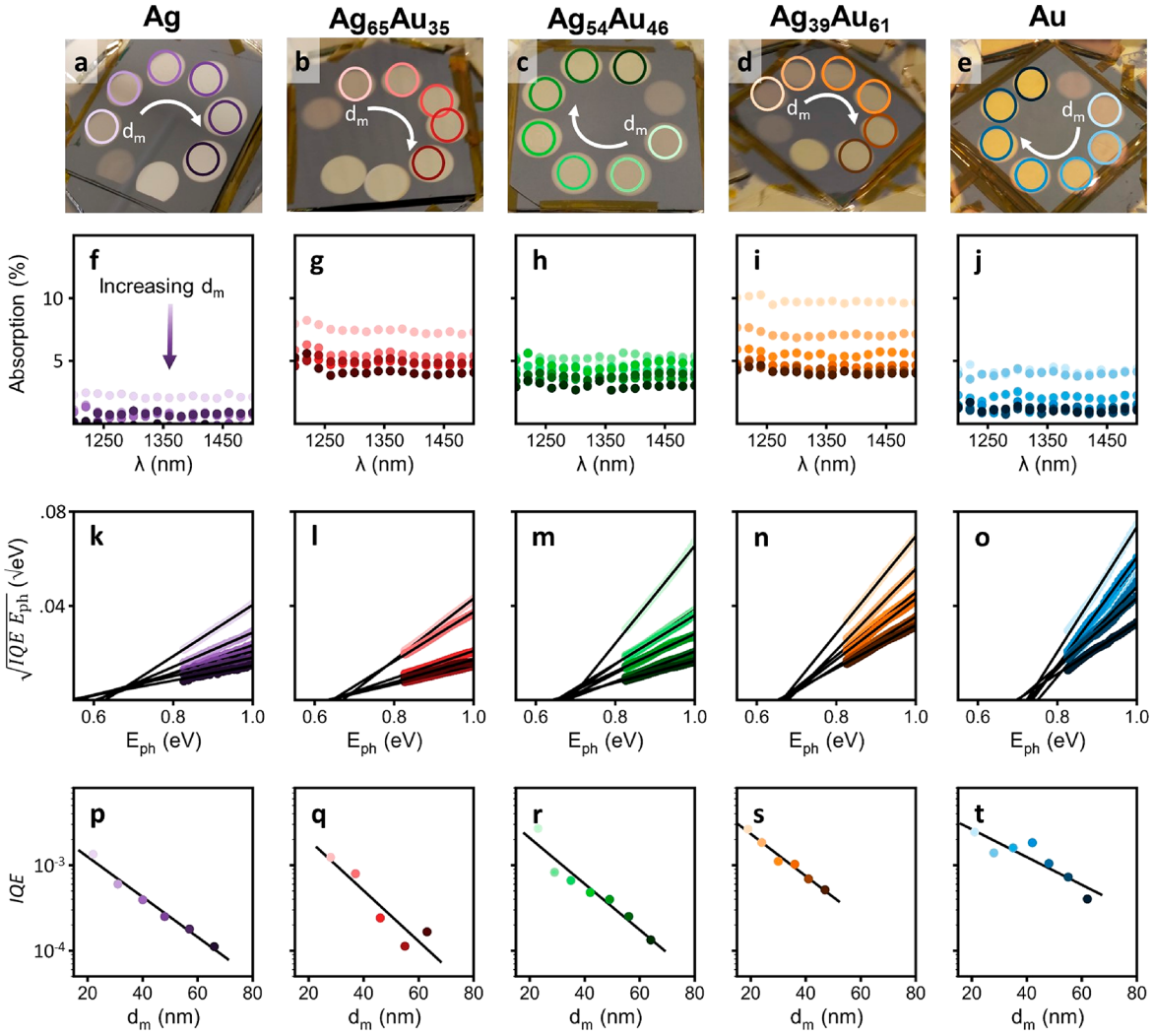

Figure 4. Measuring the hot electron attenuation length. (a–e) Optical images of the samples taken immediately after deposition. The film thicknesses are color coded from light to dark in order of increasing film thickness, d_m. (f–j) Raw data of measured absorption for all film thicknesses. (k–o) Calculated Fowler yield (circles) for all film thicknesses and their line fits (black lines) used to determine barrier height. (p–t) Logarithmic plot IQE vs film thickness for E_{ph} = 0.9 eV. The data was fit to a line (solid, black line) in order to extract the hot electron attenuation length.

Measured Device Performance. For experimental determination of absorption and photoresponse for NIR illumination, the Au, Ag, and alloy films were deposited on an *n*-type silicon substrate. Prior to depositing the metal films, Al ohmic contacts and a Si_3N_4 antireflection coating were deposited on the opposing side of each substrate. The Si_3N_4 thicknesses were 165 ± 5 nm for all samples, except for the pure Au sample, which was 145 ± 5 nm resulting in a shift in the reflection minimum from ∼1350 nm to ∼1200 nm. The metal film thicknesses were calculated from fits to the measured ellipsometry reflection and transmission data and all film thicknesses were 10 ± 2 nm. Because Au does not properly adhere to silicon, a ∼1 nm Ti adhesion layer was deposited prior to the pure Au deposition. The pure Ag and alloys did not require an adhesion layer. This was verified by inspection using a scattering electron microscope (SEM). SEM images for pure Ag and $Ag_{59}Au_{41}$ are shown in the Supporting Information, Figure S4.

While the measured absorption in Figure 3 is consistent with the calculations showing that the Au rich ($Au_{68}Ag_{32}$) alloy will have the highest absorption, pure Au has the highest measured responsivity. With the exception of pure Au, the responsivity of the photodiodes follows the trend of their measured absorption with Ag having the lowest and $Au_{68}Ag_{32}$ the highest. This leaves the question of why the Au film has the highest photoresponse when it does not present the highest absorption.

Factors that impact the photoresponse, other than absorption, are the Schottky barrier height, EDOS, and hot carrier attenuation length. According to the modified Fowler theory, the internal quantum efficiency (i.e., the ratio of extracted carriers to absorbed photons) can be approximated by $IQE \propto (E_{ph} - \Phi_B)^2/E_{ph}$, and therefore, a decrease in barrier height would lead to an increase in photoresponse.[2,30,32] A linear fit to $\sqrt{(IQE \times E_{ph})}$ can be used to determine the Schottky barrier height of each photodiode, and we find that the Au sample has the largest barrier height (Φ_B = 0.66 ± 0.02 eV, see Figure S5). As a result, the only likely explanation for the increase in photoresponse is an increase in hot carrier attenuation length in the Au (with respect to Ag and the alloys), because the EDOS distribution in this wavelength region is approximately the same for Au, Ag, and all alloys.

https://dx.doi.org/10.1021/acsphotonics.0c00140
ACS Photonics XXXX, XXX, XXX−XXX

Determining the Hot Carrier Attenuation Length. Under many circumstances, the EAL can be determined by measuring the IQE of a metal film while varying the film thickness, as discussed below. For clarity, we define the EAL as the hot electron decay length as a result of all scattering events including electron−electron and electron−phonon scattering. The EAL should not be confused with the inelastic mean free path, which only considers the average distance between electron−electron collisions. Under front illumination (i.e., illuminating the metal directly from air), the IQE as a function of film thickness, t, is given by

$$\mathrm{IQE}(t) = C\left(\frac{\alpha L}{\alpha L - 1}\right)\left(\frac{e^{-t/L} - e^{-\alpha L}}{1 - e^{-\alpha L}}\right) \tag{4}$$

where α is the optical absorption constant determined by $4\pi\kappa_m/\lambda$, L is the electron attenuation length, and C is a device-dependent constant of proportionality that depends on the quality of the Schottky junction. If the film thickness and EAL are greater than the optical penetration depth (i.e., $\alpha L > 1$ and $\alpha t > 1$, where $1/\alpha$ is the optical penetration depth), eq 4 reduces to

$$\mathrm{IQE}(t) = C\left(\frac{\alpha L}{\alpha L - 1}\right)e^{-t/L} \text{ or}$$
$$\ln(\mathrm{IQE}(t)) = \ln\left(C\left(\frac{\alpha L}{\alpha L - 1}\right)\right) - \frac{t}{L} \tag{5}$$

therefore, the slope of ln(IQE) versus thickness yields the EAL. Equations 4 and 5 have been derived, assuming the incident illumination is exponentially attenuated within the metal (i.e., the amplitude of the incident EM wave decays as $e^{-\alpha z}$, where z is the incident axis), the probability of collecting a hot electron that is excited at a distance $(t - z)$ from the Schottky interface is proportional to $e^{-(t-z)/L}$, and that the quality of the Schottky barrier (i.e., the proportionality constant, C) is the same for all films. In addition, it is assumed that the metal film is thick enough that optical reflection from the metal/semiconductor interface and multiple reflections of the hot electrons can be neglected.[33,34]

The EAL of pure Au and Ag have previously been measured using this method, but the results have varied depending upon analysis and deposition conditions. Measurements performed by Crowell et al.[34] obtained $L \sim 74$ and 44 nm for Au and Ag, respectively. Soshea et al. later pointed out that Crowell determined IQE using absorption measured from glass substrates, as opposed to the silicon substrates that were used to measure the photoresponse.[35] Because the substrate can significantly impact the absorption, these values were found to be incorrect. Soshea et al. found that the corrected EAL for Au was $L \sim 33$ nm, but they did not measure the corrected EAL for Ag. Leder et al.[36] claimed to have measured $L \sim 45$ nm for Ag, which is consistent with Crowell's measurements, however, to the best of our knowledge, Leder never officially published their measurements. Gould et al.[37] later measured $L = 20-30$ nm and 30−40 nm for Ag and Au, respectively, and Bernardi et al.[38] calculated that the EAL for low energy photons is also influenced by the crystallographic direction with the [110] direction leading to the longest EAL and [111] the lowest.

We measured the EAL of $Ag_xAu_{(100-x)}$ for x = 100, 65, 54, 39, and 0 by depositing multiple thicknesses of each metal on large Si substrates (see Figure 4a−e). An Al ohmic contact was deposited on the reverse side of each substrate. Because all of the metal films are on the same substrate, we can assume that the carrier collection properties (i.e., device resistance, resistance of the ohmic contact, etc.) will be consistent. Prior to deposition the substrates were chemically cleaned, and all metals were cosputtered through a shadow mask without breaking vacuum. Each film was simultaneously deposited on a glass substrate. Immediately after deposition, the film thicknesses and optical properties were determined from fits to measured reflection and transmission ellipsometry data and the chemical composition was measured using EDS (see results in Supporting Information, Tables S2−S4 and Figure S6). Both the ellipsometry and EDS measurements were done on the glass substrate.

The absorption, A, in each metal film was calculated from measured reflection, R, and transmission, T, on the Si substrate using $A = 1 - R - T$, Figure 4f−j. We find that, even for illumination through air, the alloys absorb ∼5−10% more than the pure metals. Note that we exclude the thinnest film thickness on all samples from the measurements because these film thicknesses are below the optical penetration depth (i.e., $1/\alpha$) and therefore does not satisfy the $\alpha t > 1$ requirement for eq 5. We also excluded the maximum film thicknesses for Ag, $Ag_{65}Au_{35}$, and $Ag_{39}Au_{61}$ because the films were too thick, causing the photoresponse to be too low to measure.

The IQE was calculated from the measured responsivity and absorption, which can be determined by

$$\mathrm{IQE}(E_{ph}) = \frac{E_{ph}}{q} \times \frac{R}{A} \tag{6}$$

where E_{ph} is the photon energy, q is the charge of an electron, R is the measured responsivity in units of ampere/watt and A is the measured absorption. The responsivity was measured at zero bias and the IV curves for each material and thickness can be found in Figure S7. The measured absorption for the thicker Ag films is below the signal-to-noise ratio of our measurements; however, the measured absorption closely matches the expected absorption calculated using the optical properties determined from ellipsometry (see Figure S8). We therefore use the calculated absorption for determining the IQE for each Ag film thickness. For all other alloys, the IQE was determined from the measured absorption using a Savitzky−Golay filter to reduce the noise in the measurements (see Figure S9 for filtered absorption). The source of the noise in the measurements was predominantly due to laser power fluctuations.

The barrier height for each photodiode was determined using a linear fit to the Fowler yield, $\sqrt{(\mathrm{IQE} \times E_{ph})}$, for each photodiode. The variation in the barrier heights can be seen as the x-intercept of the linear fits in Figure 4k−o. The barrier heights for each metal are consistent with relative differences <5%, except for pure Ag which has a larger spread (<9%). The average barrier height for each metal increases almost linearly from 0.58 to 0.72 eV with increasing Au content, Figure S10a. When comparing the calculated barrier heights from the fitting the Fowler yield to those from fitting the IV curves, we find good agreement, further validating these measurements. This data along with the ideality factors for each material and thickness can be found in Tables S5−S9.

Maintaining the slope from the linear fits to the Fowler yield, the IQE for each film thickness was determined using the average barrier height for each metal at a photon energy of 0.9

https://dx.doi.org/10.1021/acsphotonics.0c00140
ACS Photonics XXXX, XXX, XXX−XXX

eV, Figure 4p–t. The EAL is determined by the slope of the linear fit to ln(IQE(t)). The extracted EAL is shown in Figure 5. We find that Au has the highest attenuation length and

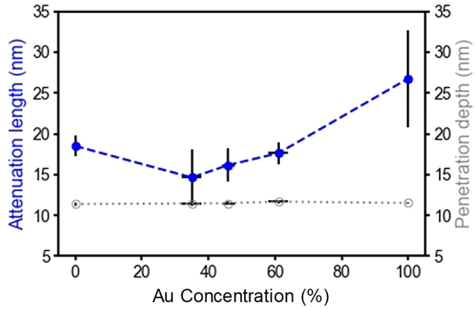

Figure 5. Measured hot electron attenuation length varying Au concentration compared to the optical penetration depth.

$Ag_{65}Au_{35}$ has the lowest, however, $Ag_{65}Au_{35}$ and $Ag_{54}Au_{46}$ have similar EAL's within error. The error is defined as one standard deviation error as determined by the covariance matrix in the linear fit to ln(IQE(t)). Au has the largest error because it has poor adhesion to Si resulting in reduced film quality, but the measured EAL is consistent with previously reported results within error. AFM topography scans verified that Au has the largest crystal sizes and surface roughness resulting in poor film quality (Figures S10 and S11). The thin film Au device shown in Figure 3 has significantly greater performance as a result of improved film quality because of the Ti adhesion layer.

While alloys with >70% Au may result in higher EAL compared to pure Ag, all the measured alloys have reduced EAL compared to the pure metals. There are many material dependent factors that impact the EAL, including the Fermi velocity of the electron gas, plasma frequency, atomic radius and crystal orientation; however, most of these factors are similar between the Au and Ag films with the exception of the plasma frequency.[39−41] (Note that X-ray diffraction (see Figure S12) shows that the preferred crystal orientation for all the metals was [111] with only Ag showing a small percentage of crystals in the [100] direction.) If only the plasma frequency was impacting the EAL of the alloys, the EAL would likely increase almost linearly with increasing Au concentration. Because this is not the trend that the data shows, the most likely factor impacting the EAL of the Ag-Au alloys is an increase in scattering sites for the electrons as opposed to an intrinsic electrical property of the metals.

Enhanced electron scattering can arise from grain boundaries and surface roughness. In our case, we find that the most significant contributing factor is grain boundary scattering. Using X-ray diffraction, we found that $Ag_{54}Au_{46}$ and $Ag_{65}Au_{35}$ have the smallest and second smallest grains, respectively (Figures S10b and S12). Reduced grain sizes result in a shorter path length between electron scattering events resulting in a decrease in electron mean free path. Even the Drude dampening, which is also influenced by electron scattering, follows the trend of the metal grain size (Figure S9b). In addition, AFM surface scans show that the alloys have lower surface roughness and therefore are less likely to be impacted by surface scattering than the pure metals (Figure S10c).

Because the EAL appears to be significantly impacted by the grain boundaries, it is likely possible to improve the EAL by finding methods of increasing the grain sizes. The EAL could also be lower in these films compared to their maximum possible EAL because of the preferred crystal orientation.[38] Increasing the grain size and reorienting the crystals to the [110] or [100] directions could be accomplished through thermal evaporation of a prealloyed target, annealing the samples after deposition, or exploring other deposition methods such as pulsed laser deposition. However, a decrease in electron scattering will also result in a decrease in Drude dampening and will subsequently reduce the thin film absorption. Rioux's model shows that the alloys will always have higher intrinsic defect scattering compared to the pure metals suggesting that their EAL will not surpass pure Au. In fact, the difference between the expected absorption for the alloys and our measured absorption in Figure 1c is likely because of enhanced scattering from grain boundaries resulting from cosputtered deposition. Therefore, it is reasonable to assume that increasing grain sizes would only reduce the thin film absorption by ∼10%. As a result, it may be possible to increase the EAL of the alloys to lengths longer than pure Ag.

CONCLUSION

In summary, we have shown that Ag_xAu_{100-x} alloys have 10–20% higher absorption compared to the pure metals in the NIR. Yet, even though their hot carrier distributions are equivalent, pure Au outperforms Ag and the alloys for efficient hot carrier photodetection. The beneficial performance of Au appears to be correlated with electron scattering from grain boundaries; because Au has the largest grain boundaries it has the lowest volume of scattering sites and therefore the longest EAL. We observe an inverse relationship between the Drude dampening (i.e., the imaginary part of the dielectric function) and the EAL, which is expected because both are impacted by electron scattering. Therefore, it may be possible to predict whether alloying will reduce or increase the EAL with respect to pure metals through simply measuring the imaginary part of the dielectric function. Further investigation is required to find an alloy that has high absorption, ideal hot carrier distribution, and a long EAL. Because metals such as Pt and Cr have high absorption,[13] it may be possible to find alloys with these metals that will increase their EAL. Gong and Munday showed that it is possible to improve the hot hole distribution for efficient carrier injection in Pt through alloying with Au.[8] Further, alloys involving three or more metals may provide additional opportunities to customize both the material's optical and electrical response and to maximize the hot carrier generation and injection, leading to higher efficiencies and new photodetector architectures.

METHODS

Sample Fabrication. All photodiodes were fabricated on 370 μm thick, double-sided polished, ⟨100⟩ n-type silicon wafers (<1 Ω cm). The wafers were chemically cleaned using piranha (3:1 sulfuric acid (H_2SO_4) and hydrogen peroxide (H_2O_2)) and a buffered oxide etch (BOE) prior to depositing a thin Al ohmic contact through a shadow mask using electron beam evaporation (Å). The Al contacts were annealed at 425°C in forming gas (96% Ar and 4% H_2).

All alloys were cosputtered using pure metal targets with >99.99% purity. Immediately prior to deposition, a thick photoresist layer was spin-coated over the entire Si surface with the Al contacts. The opposing side of the substrates were then cleaned with BOE to remove the oxide growth resulting

https://dx.doi.org/10.1021/acsphotonics.0c00140
ACS Photonics XXXX, XXX, XXX−XXX

from the Al contact anneal. The metals in Figure 3 were sputtered through a shadow mask on 1 cm^2 *n*-Si wafers using an AJA ATC 1800 sputtering unit. The metals for the EAL (Figures 4 and 5) were sputtered through a circular shadow mask with 0.3 in. diameter on a 3.2 × 3.2 cm^2 *n*-Si substrate using an AJA ATC Orion 8 sputtering unit. The shadow mask was rotated between depositions without breaking vacuum in order to prevent oxidation.

Material Characterization. For each metal deposition, a glass slide was included in the deposition to determine the thickness, refractive index, and alloy composition of the deposited metal. All material refractive indices and thicknesses were determined using a J.A. Woollam M-2000D Spectroscopic Ellipsometer, 8″ (190−1700 nm). The alloy composition was measured in a Hitachi S-3400 variable pressure SEM fitted with an EDS analyzer. The measurements were taken using a 6 kV beam with 75 A current.

Surface roughness measurements were taken in a Cypher Atomic Force Microscope (Asylum Research) under ambient atmosphere. For each metal, three 1 × 1 μm scans were taken. The reported roughnesses are all root-mean-square roughnesses (RMS) and are calculated by taking the RMS value of each line of the AFM image and taking the median of these values.

Optical and Electrical Measurements. Absorption measurements in Figure 3 were performed using a 6 in. integrating sphere (Labsphere RTC-060) with an illumination at ∼12° incidence. Two Ge photodiodes were used to measure the light intensity inside the integrating sphere and to monitor power fluctuations of the incident beam. Specific NIR wavelengths were selected from a supercontinuum source (Fianium WhiteLase) using an acousto-optic tunable filter (AOTF), and the incident light was chopped using a rotating disk chopper. The signals from the photodiodes were measured using a SR830 lock-in amplifier with the reference frequency matched to the frequency of the optical chopper. The uncertainty of the measured absorption is ±0.5%.

To determine the responsivity of the fabricated photodiodes, the samples were mounted on a vertical stage with copper probes forming an electrical contact to the Al ohmic and Ag-Au contacts. The incident light was focused on the sample at normal incidence and the power incident on the sample was determined by a calibrated Ge photodiode. The signals from the sample and each photodiode were measured using a SR830 lock-in amplifier. All measurements were recorded at 0 V bias. There is a 2−3% uncertainty in the measured responsivity.

The absorption of the alloys for the EAL measurements were measured on the same stage used to measure responsivity. The absorption was determined from measuring the transmission and reflection. The transmission was measured by mounting a calibrated Ge photodiode directly behind the sample aligned to the incident beam. The reflection was measured by reflecting the incident light off the sample at a near-normal incident angle of 10 ± 2° into a calibrated Ge photodiode. The reflected and transmitted power was compared to the total power hitting the sample, as measured by a reference calibrated Ge photodiode to determine the percent reflection and transmission.

Density Functional Theory. The DFT calculations were performed on a supercell containing 108 atoms of Au and Ag in different concentrations. The disordered alloys were obtained by constructing a special quasi-random structure converging the correlation function of the disordered alloy up to the third nearest neighbors, using the ATAT package.[42] Using these coordinates, the density of states and band structures were obtained, calculated with the SIESTA code,[43] with a double-ζ atomic basis set with polarization orbitals, norm conserving relativistic pseudo potentials, and the PBE-flavor of the generalized gradient approximation (GGA) for the exchange and correlation potential. The structures were fully relaxed to a target pressure of 0 kbar, a maximum of 0.01 eV/$Å^{-1}$ using a 500 Ry real space mesh cutoff, and a 30 × 30 × 30 (7 × 7 × 7) *k*-point grid for the pure metals (alloys). In the case of the density of states, the k-point grid was increased 3-fold. Finally, the unfolding of the bands follows a generalization of the work by Mayo et al.[44] for orbital-projected bands.

■ ASSOCIATED CONTENT

Supporting Information

The Supporting Information is available free of charge at https://pubs.acs.org/doi/10.1021/acsphotonics.0c00140.

EDS results, modeled and measured refractive index of AuAg alloys, quasi-random super cell arrangement used for DFT calculations, hot carrier distribution for various wavelengths for the alloys and pure metals, SEM images of Ag and $Ag_{59}Au_{41}$ deposited on silicon, fits to Fowler yield, recorded *IV* curves for each alloy thickness, ideality factors and barrier heights for each film thickness, optical properties of all metal films, reflectivity, transmission, and absorption for all metal films, barrier heights, crystal size, and RMS roughness of metal films, and X-ray diffraction data for all alloys (PDF)

■ AUTHOR INFORMATION

Corresponding Author

Jeremy N. Munday − *Department of Electrical and Computer Engineering and Institute for Research in Electronics and Applied Physics, University of Maryland, College Park, Maryland 20742, United States; Department of Electrical and Computer Engineering, University of California, Davis, California 95616, United States;* orcid.org/0000-0002-0881-9876; Email: jnmunday@ucdavis.edu

Authors

Lisa J. Krayer − *Department of Electrical and Computer Engineering and Institute for Research in Electronics and Applied Physics, University of Maryland, College Park, Maryland 20742, United States;* orcid.org/0000-0001-9133-226X

Kevin J. Palm − *Institute for Research in Electronics and Applied Physics and Department of Physics, University of Maryland, College Park, Maryland 20742, United States;* orcid.org/0000-0003-4066-4584

Chen Gong − *Institute for Research in Electronics and Applied Physics and Department of Materials Science and Engineering, University of Maryland, College Park, Maryland 20742, United States;* orcid.org/0000-0003-3302-7675

Alberto Torres − *Instituto de Física Teórica, São Paulo State University (UNESP), São Paulo, SP 01140-070, Brazil*

Cesar E. P. Villegas − *Instituto de Física Teórica, São Paulo State University (UNESP), São Paulo, SP 01140-070, Brazil; Departamento de Ciências, Universidad Privada del Norte, Lima 15314, Peru;* orcid.org/0000-0003-2675-1331

https://dx.doi.org/10.1021/acsphotonics.0c00140
ACS Photonics XXXX, XXX, XXX−XXX

Alexandre R. Rocha − *Instituto de Física Teórica, São Paulo State University (UNESP), São Paulo, SP 01140-070, Brazil;* orcid.org/0000-0001-8874-6947

Marina S. Leite − *Institute for Research in Electronics and Applied Physics and Department of Materials Science and Engineering, University of Maryland, College Park, Maryland 20742, United States; Department of Material Science and Engineering, University of California, Davis, California 95616, United States;* orcid.org/0000-0003-4888-8195

Complete contact information is available at: https://pubs.acs.org/10.1021/acsphotonics.0c00140

Funding

This material is based on work supported by the National Science Foundation (NSF) CAREER Grant No. ECCS-1554503, the NSF DMR award No. 16-09414 and No. 20-16617, and the Office of Naval Research YIP Award under Grant No. N00014-16-1-2540. L.J.K. is supported by an NSF Graduate Research Fellowship (DGE 1322106, ECCS-1554503) and an Ann G. Wylie Dissertation Fellowship. K.J.P. is supported by a National Defense Science and Engineering Graduate Fellowship. A.T. and A.R.R. acknowledge support by Fundação de Amparo à Pesquisa do Estado de São Paulo (FAPESP), Grant Nos. 2016/01343-7, 2017/02317-2, and 2018/12545-5. C.G. was supported by the Harry K. Wells fellowship.

Notes

The authors declare no competing financial interest.

■ ACKNOWLEDGMENTS

We thank the FabLab at the Maryland Nanocenter for access to all fabrication equipment, including, but not limited to, the e-beam evaporator, the AJA sputter deposition tool, and the Woollam Spectroscopic Ellipsometer. This research was supported by computational resources supplied by the Center for Scientific Computing (NCC/GridUNESP) of the São Paulo State University (UNESP) and the National Laboratory for Scientific Computing (LNCC/MCTI, Brazil) via the SDumont supercomputer.

■ REFERENCES

(1) Dalal, V. L. Simple Model for Internal Photoemission. *J. Appl. Phys.* **1971**, *42* (6), 2274−2279.
(2) Leenheer, A. J.; Narang, P.; Lewis, N. S.; Atwater, H. A. Solar Energy Conversion via Hot Electron Internal Photoemission in Metallic Nanostructures: Efficiency Estimates. *J. Appl. Phys.* **2014**, *115* (13), 134301.
(3) Li, W.; Valentine, J. Metamaterial Perfect Absorber Based Hot Electron Photodetection. *Nano Lett.* **2014**, *14* (6), 3510−3514.
(4) Tanaka, A.; Teramura, K.; Hosokawa, S.; Kominami, H.; Tanaka, T. Visible Light-Induced Water Splitting in an Aqueous Suspension of a Plasmonic Au/TiO 2 Photocatalyst with Metal Co-Catalysts. *Chem. Sci.* **2017**, *8* (4), 2574−2580.
(5) Brolo, A. G. Plasmonics for Future Biosensors. *Nat. Photonics* **2012**, *6* (11), 709−713.
(6) Anker, J. N.; Hall, W. P.; Lyandres, O.; Shah, N. C.; Zhao, J.; Van Duyne, R. P. Biosensing with Plasmonic Nanosensors. *Nat. Mater.* **2008**, *7* (6), 442−453.
(7) Lal, S.; Link, S.; Halas, N. J. Nano-Optics from Sensing to Waveguiding. *Nat. Photonics* **2007**, *1* (11), 641−648.
(8) Gong, T.; Munday, J. N. Materials for Hot Carrier Plasmonics [Invited]. *Opt. Mater. Express* **2015**, *5* (11), 2501.
(9) Scales, C.; Berini, P. Thin-Film Schottky Barrier Photodetector Models. *IEEE J. Quantum Electron.* **2010**, *46* (5), 633−643.
(10) Sundararaman, R.; Narang, P.; Jermyn, A. S.; Goddard, W. A., III; Atwater, H. A. Theoretical Predictions for Hot-Carrier Generation from Surface Plasmon Decay. *Nat. Commun.* **2014**, *5* (1), 5788.
(11) Valenti, M.; Venugopal, A.; Tordera, D.; Jonsson, M. P.; Biskos, G.; Schmidt-Ott, A.; Smith, W. A. Hot Carrier Generation and Extraction of Plasmonic Alloy Nanoparticles. *ACS Photonics* **2017**, *4* (5), 1146−1152.
(12) West, P. R.; Ishii, S.; Naik, G. V.; Emani, N. K.; Shalaev, V. M.; Boltasseva, A. Searching for Better Plasmonic. *Materials. Laser Photon. Rev.* **2010**, *4* (6), 795−808.
(13) Krayer, L. J.; Tennyson, E. M.; Leite, M. S.; Munday, J. N. Near-IR Imaging Based on Hot Carrier Generation in Nanometer-Scale Optical Coatings. *ACS Photonics* **2018**, *5* (2), 306−311.
(14) Mondolfo, L. F. *Aluminum Alloys: Structure and Properties*; Butterworth & Co. Ltd., 1979.
(15) Cortie, M. B.; McDonagh, A. M. Synthesis and Optical Properties of Hybrid and Alloy Plasmonic Nanoparticles. *Chem. Rev.* **2011**, *111* (6), 3713−3735.
(16) Dias, M. R. S.; Gong, C.; Benson, Z. A.; Leite, M. S. Lithography-Free, Omnidirectional, CMOS-Compatible AlCu Alloys for Thin-Film Superabsorbers. *Adv. Opt. Mater.* **2018**, *6* (2), 1−8.
(17) McClure, J. P.; Boltersdorf, J.; Baker, D. R.; Farinha, T. G.; Dzuricky, N.; Villegas, C. E. P.; Rocha, A. R.; Leite, M. S. Structure-Property-Performance Relationship of Ultrathin Pd-Au Alloy Catalyst Layers for Low-Temperature Ethanol Oxidation in Alkaline Media. *ACS Appl. Mater. Interfaces* **2019**, *11* (28), 24919−24932.
(18) Gong, C.; Dias, M. R. S.; Wessler, G. C.; Taillon, J. A.; Salamanca-Riba, L. G.; Leite, M. S. Near-Field Optical Properties of Fully Alloyed Noble Metal Nanoparticles. *Adv. Opt. Mater.* **2017**, *5* (1), 1600568.
(19) Link, S.; Wang, Z. L.; El-Sayed, M. A. Alloy Formation of Gold−Silver Nanoparticles and the Dependence of the Plasmon Absorption on Their Composition. *J. Phys. Chem. B* **1999**, *103* (18), 3529−3533.
(20) Gong, C.; Leite, M. S. Noble Metal Alloys for Plasmonics. *ACS Photonics* **2016**, *3* (4), 507−513.
(21) Mallin, M. P.; Murphy, C. J. Solution-Phase Synthesis of Sub-10 Nm Au−Ag Alloy Nanoparticles. *Nano Lett.* **2002**, *2* (11), 1235−1237.
(22) Rivory, J. Comparative Study of the Electronic Structure of Noble-Metal-Noble-Metal Alloys by Optical Spectroscopy. *Phys. Rev. B* **1977**, *15* (6), 3119−3135.
(23) Sinzig, J.; Radtke, U.; Quinten, M.; Kreibig, U. Binary Clusters: Homogeneous Alloys and Nucleus-Shell Structures. *Z. Phys. D: At., Mol. Clusters* **1993**, *26* (1−4), 242−245.
(24) Rioux, D.; Vallières, S.; Besner, S.; Muñoz, P.; Mazur, E.; Meunier, M. An Analytic Model for the Dielectric Function of Au, Ag, and Their Alloys. *Adv. Opt. Mater.* **2014**, *2* (2), 176−182.
(25) Gaudry, M.; Lermé, J.; Cottancin, E.; Pellarin, M.; Vialle, J.-L.; Broyer, M.; Prével, B.; Treilleux, M.; Mélinon, P. Optical Properties of (AuxAg1-x)n Clusters Embedded in Alumina: Evolution with Size and Stoichiometry. *Phys. Rev. B: Condens. Matter Mater. Phys.* **2001**, *64* (8), 085407.
(26) Yakubovsky, D. I.; Arsenin, A. V.; Stebunov, Y. V.; Fedyanin, D. Y.; Volkov, V. S. Optical Constants and Structural Properties of Thin Gold Films. *Opt. Express* **2017**, *25* (21), 25574.
(27) Born, M.; Wolf, E. *Principles of Optics*, 7th ed.; Cambridge University Press: Cambridge, 1999.
(28) Zunger, A.; Wei, S.-H.; Ferreira, L. G.; Bernard, J. E. Special Quasirandom Structures. *Phys. Rev. Lett.* **1990**, *65* (3), 353−356.
(29) Gong, C.; Kaplan, A.; Benson, Z. A.; Baker, D. R.; McClure, J. P.; Rocha, A. R.; Leite, M. S. Band Structure Engineering by Alloying for Photonics. *Adv. Opt. Mater.* **2018**, *6* (17), 1800218.
(30) Sze, S. M.; Ng, K. K. *Physics of Semiconductor Devices*, 3rd ed.; Wiley, 2006.
(31) Michaelson, H. B. The Work Function of the Elements and Its Periodicity. *J. Appl. Phys.* **1977**, *48* (11), 4729−4733.

(32) Fowler, R. H. The Analysis of Photoelectric Sensitivity Curves for Clean Metals at Various Temperatures. *Phys. Rev.* **1931**, *38* (1), 45−56.
(33) Crowell, C. R.; Sze, S. M. Hot-Electron Transport and Electron Tunneling in Thin Film Structures. In *Physics of Thin Films*; Hass, G., Thun, R. E., Eds.; Academic Press: New York, NY, 1967; Vol. *4*, pp 325−371.
(34) Crowell, C. R.; Spitzer, W. G.; Howarth, L. E.; Labate, E. E. Attenuation Length Measurements of Hot Electrons in Metal Films. *Phys. Rev.* **1962**, *127* (6), 2006−2015.
(35) Soshea, R. W.; Lucas, R. C. Attenuation Length of Hot Electrons in Gold. *Phys. Rev.* **1965**, *138* (4A), A1182−A1188.
(36) Leder, L. B.; Lasser, M. E.; Rudolph, D. C. Attenuation of Photoexcited Electrons in Cu and Holes in Al. *Appl. Phys. Lett.* **1964**, *5* (11), 215−217.
(37) Gould, R. D.; Hogarth, C. A. In-Situ Attenuation Length Measurements in Gold, Silver and Copper Films, Using Electroformed Emission Structures. *Int. J. Electron.* **1988**, *64* (2), 283−288.
(38) Bernardi, M.; Mustafa, J.; Neaton, J. B.; Louie, S. G. Theory and Computation of Hot Carriers Generated by Surface Plasmon Polaritons in Noble Metals. *Nat. Commun.* **2015**, *6* (1), 7044.
(39) Ding, Z.-J.; Shimizu, A. R. Rapid #: −12390199 A Monte Carlo Modeling of Electron Interaction with Solids Including Cascade Secondary Electron Production. *Scanning* **1996**, *18*, 92−113.
(40) Gall, D. Electron Mean Free Path in Elemental Metals. *J. Appl. Phys.* **2016**, *119* (8), 085101.
(41) Quinn, J. J. Range of Excited Electrons in Metals*. *Phys. Rev.* **1962**, *126* (4), 1453−1457.
(42) van de Walle, A.; Tiwary, P.; de Jong, M.; Olmsted, D. L.; Asta, M.; Dick, A.; Shin, D.; Wang, Y.; Chen, L.-Q.; Liu, Z.-K. Efficient Stochastic Generation of Special Quasirandom Structures. *CALPHAD: Comput. Coupling Phase Diagrams Thermochem.* **2013**, *42*, 13−18.
(43) Soler, J. M.; Artacho, E.; Gale, J. D.; García, A.; Junquera, J.; Ordejón, P.; Sánchez-Portal, D. The SIESTA Method for Ab Initio Order- N Materials Simulation. *J. Phys.: Condens. Matter* **2002**, *14* (11), 2745−2779.
(44) Mayo, S. G.; Yndurain, F.; Soler, J. M. Band Unfolding Made Simple. *J. Phys.: Condens. Matter* **2020**, *32* (20), 205902.

https://dx.doi.org/10.1021/acsphotonics.0c00140
ACS Photonics XXXX, XXX, XXX−XXX